There are amendments to this paper

npj Computational Materials

www.nature.com/npjcompumats

ARTICLE OPEN

Possible ground states and parallel magnetic-field-driven phase transitions of collinear antiferromagnets

Hai-Feng Li[1]

Understanding the nature of all possible ground states and especially magnetic-field-driven phase transitions of antiferromagnets represents a major step towards unravelling the real nature of interesting phenomena such as superconductivity, multiferroicity or magnetoresistance in condensed-matter science. Here a consistent mean-field calculation endowed with antiferromagnetic (AFM) exchange interaction (J), easy axis anisotropy (γ), uniaxial single-ion anisotropy (D) and Zeeman coupling to a magnetic field parallel to the AFM easy axis consistently unifies the AFM state, spin-flop (SFO) and spin-flip transitions. We reveal some mathematically allowed exotic spin states and fluctuations depending on the relative coupling strength of (J, γ and D). We build the three-dimensional (J, γ and D) and two-dimensional (γ and D) phase diagrams clearly displaying the equilibrium phase conditions and discuss the origins of various magnetic states as well as their transitions in different couplings. Besides the traditional first-order type one, we unambiguously confirm an existence of a second-order type SFO transition. This study provides an integrated theoretical model for the magnetic states of collinear antiferromagnets with two interpenetrating sublattices and offers a practical approach as an alternative to the estimation of magnetic exchange parameters (J, γ and D), and the results may shed light on nontrivial magnetism-related properties of bulks, thin films and nanostructures of correlated electron systems.

npj Computational Materials (2016) **2,** 16032; doi:10.1038/npjcompumats.2016.32; published online 14 October 2016

INTRODUCTION

Nontrivial magnetism-related properties such as superconductivity, multiferroicity or magnetoresistance of correlated electron systems[1–5] continue to be exciting fields of research in both theoretical and experimental condensed-matter science. Such experimental observations pose their specific challenges to a complete theoretical framework.[6–9] These macroscopic functionalities may intricately connect with quantum phase transitions, strictly speaking, occurring at zero temperature and corresponding fluctuations on the border of distinct phases of a quantum phase transition.[10–18] Such quantum phase transitions and fluctuations can be realised and finely tuned by a non-temperature control parameter such as pressure, chemical substitution or magnetic field. A complete understanding of such experimental observations necessaries a full reveal of all possible ground states and especially magnetic-field-driven phase transitions and fluctuations of magnets, which is the central topic of our present study focusing on a theoretical calculation accommodating competitive and cooperative interactions[19–23] for collinear antiferromagnets.

For a collinear antiferromagnet below the Néel temperature, when a magnetic field ($\boldsymbol{B}$) applied along the antiferromagnetic (AFM) easy axis reaches a critical value (B_{SFO}), the AFM sublattice spins suddenly rotate 90° so that they are perpendicular to the original AFM easy axis. This is the traditional spin-flop (SFO) transition, typically a first-order (FO) type in character. After this, the flopped spins gradually tilt toward the field direction with increasing field strength ($B > B_{SFO}$) until they are completely aligned at a sufficiently high magnetic field (B_{SFI}), which is the so-called spin-flip (SFI) transition. These magnetic-field-driven magnetic phase transitions of collinear antiferromagnets are schematically sketched in Figure 1.

Experimentally, identifying the nature of a SFO transition, FO or second order (SO) remains a major challenge in condensed-matter science mainly due to the technically unavoidable effect of misalignment between the relevant AFM easy axis and an applied-field direction. Néel for the first time proposed theoretically the possibility for a SFO transition in 1936.[24] Subsequently, it was observed experimentally in a $CuCl_2{\cdot}2H_2O$ single crystal.[25] Since then, the SFO phase transition has been extensively investigated, and the corresponding phenomenological theory has been comprehensively developed, generally confirming that it is of FO in nature.[26–41] However, most of the reported 'sharp' SFO transitions[34,42,43] display no magnetic hysteresis effect characteristic of a FO phase transition. This was attributed either to a low magnetic anisotropy[34,43] or to a softening of surface magnons.[44] In addition, some FO SFO transitions are obviously continuous occurring in a broad magnetic-field range, which was attributed either to a domain effect resulting from an inhomogeneous character of the diluted systems or to a misalignment of applied magnetic field with regard to the AFM easy axis.[32,45,46] On the other hand, such kind of continuous magnetic phase transitions,[47,48] the absence of magnetic hysteresis and the experimental observation of a possible intermediate phase in the SFO compound $CoBr_2{\cdot}6[0.48D_2O, 0.52H_2O]$,[49,50] cast considerable doubt on the nature of SFO transitions and in addition may indicate a SO-type phase transition. Experimentally, it is not easy to distinguish the origin of a virtual SO-type SFO transition because the allowed small misalignment for a FO SFO transition[32,45,46] is usually beyond the present experimental accuracy, and any larger misalignment may change a FO-type

[1]Institute of Applied Physics and Materials Engineering, Faculty of Science and Technology, University of Macau, Avenida da Universidade, Taipa, Macau, China.
Correspondence: H-F Li (haifengli@umac.mo)
Received 28 October 2015; revised 1 September 2016; accepted 7 September 2016

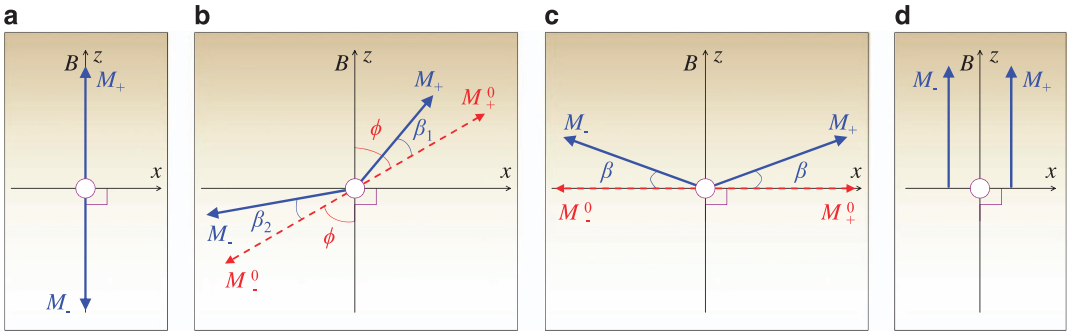

Figure 1. Schematic SFO and SFI transitions of a collinear two-sublattice antiferromagnet. (**a**) In a normal AFM state, the AFM easy axis $M^0_- M^0_+$ coincides with the localised sublattice moments M_+ and M_- (supposed to be along the z axis). (**b**) A SO SFO transition. ϕ denotes an angle of the AFM easy direction away from the z axis. β_1 and β_2 correspond to the angles of sublattice moments M_+ and M_- away from the $M^0_- M^0_+$ axis, respectively. (**c**) When $\phi = 90°$, the sublattice moments are flopped at B_{SFO} and then tilted away from the x axis by an angle β. (**d**) The sublattice moments M_+ and M_- are completely aligned along the $\boldsymbol{B}$ direction in a strong enough magnetic field B_{SFI}.

into a SO-type broadening SFO transition. Although early theoretical calculations predicted an intermediate regime bordering with the AFM and spin-flopped states,[51–53] these either have not yet been confirmed based on the principle of minimum total potential free energy, or the used theoretical model overlooked the singe-ion anisotropy that is of very important for lanthanides and actinides.[54–58] In addition, a rotating ferromagnetic (FM) phase was also predicted for a SFO antiferromagnet while increasing magnetic field along the AFM easy axis.[51,59] However, such kind of unusual magnetic phase has never been observed experimentally, which renders the validity of the phase undecided.

Herein, the magnetic-field-driven SFO and SFI phase transitions of localised collinear antiferromagnets with two sublattices are explored with a mean-field theoretical calculation. Our model unifies all possible magnetic ground states and reveals some interesting magnetic phase transitions and coexistences of some of the magnetic states. This study unambiguously reveals a SO-type SFO transition via comparing numerically the relative sublattice-moment-related free energy. We conclusively rule out the possibility for a rotating FM-like magnetic state.[51] This model calculation consistently covers all possible magnetic-field-driven magnetic states of collinear antiferromagnets. We further deduce an alternative to the estimation of magnetic exchange parameters (J, γ and D).

RESULTS

Derived equilibrium magnetic states

Possible equilibrium magnetic states can be derived from different combinations of the FO partial differential equations, i.e., $\frac{\partial E}{\partial \beta} = \frac{\partial E}{\partial \phi} = 0$ (β corresponds to the angle of AFM sublattice moments M_+ and M_- away from the $M^0_- M^0_+$ axis and ϕ denotes an angle of the AFM easy direction away from the z axis) with Equation (28):

$$\begin{cases} 2DM_0 \sin\phi \ \cos(2\beta) + \gamma M_0 \sin\phi - B\sin\beta = 0, \\ 2JM_0 \sin\beta + 2DM_0 \cos(2\phi)\sin\beta \\ +\gamma M_0 \sin\beta - B\sin\phi = 0; \end{cases} \quad (1)$$

$$\begin{cases} \cos\phi = 0, \\ 2JM_0 \sin\beta + 2DM_0 \cos(2\phi)\sin\beta \\ +\gamma M_0 \sin\beta - B\sin\phi = 0; \end{cases} \quad (2)$$

$$\begin{cases} 2DM_0 \sin\phi\cos(2\beta) + \gamma M_0 \sin\phi - B\sin\beta = 0, \\ \cos\beta = 0; \end{cases} \quad (3)$$

$$\begin{cases} \cos\phi = 0, \\ \cos\beta = 0. \end{cases} \quad (4)$$

In the following, the four combinations (1–4) will tentatively be solved, and the resulting solutions will be connected with physical meanings accordingly.

(i) First, the combination (1) involves the most formidable challenge, and one can obtain ultimately two solutions:

$$\begin{array}{l} (A)\ \sin\phi = \sin\beta = 0, \ \text{i.e.,}\ \ \phi = \beta = 0; \\ (B)\ \sin\phi = \delta\sin\beta, \ \ \text{where} \end{array} \quad (5)$$

$$\begin{array}{l} \sin\beta = \sqrt{\frac{\delta M_0(2D+\gamma) - B}{4\delta M_0 D}}\ \text{and} \\ \delta = \sqrt{\frac{2J+2D+\gamma}{2D+\gamma}}. \end{array} \quad (6)$$

The former case (A) is associated with an AFM ground state as shown in Figure 1a, whereas the latter case (B) signifies a correlated change of ϕ with β. As shown in Figure 1, $0° \leqslant \phi \leqslant 90°$. Consequently, there are two boundary magnetic fields corresponding to the second solution of the combination (1) (i.e., a SFO transition). When $\phi = 0$, $\sin\phi = \delta \sin\beta = 0$. One can deduce that the initial magnetic field for the beginning of the SFO transition

$$B_{SFOB} = M_0\sqrt{(2D+\gamma)(2J+2D+\gamma)}. \quad (7)$$

When $\phi = \frac{\pi}{2}$, $\delta \sin\beta = 1$, therefore, the final magnetic field for the ending of the SFO transition

$$B_{SFOF} = M_0(2J-2D+\gamma)\sqrt{\frac{2D+\gamma}{2J+2D+\gamma}}. \quad (8)$$

When $B_{SFOB} \geqslant B_{SFOF}$, one can derive the precondition of a FO SFO transition: $D \geqslant 0$ and $2D+\gamma > 0$. On the other hand, when $B_{SFOB} < B_{SFOF}$, i.e., $-\frac{1}{2}\gamma < D < 0$, a surprising SO SFO transition occurs spontaneously, which originates from a negative single-ion anisotropy (relative to the magnetic interaction) that is additionally restricted to a certain range by the anisotropic exchange interaction (γ).

(ii) The combination (2) implies that

$$\begin{array}{l} \phi = \frac{\pi}{2}, \ \text{and} \\ \sin\beta = \frac{B}{M_0(2J-2D+\gamma)}, \end{array} \quad (9)$$

which corresponds to the process of a SFI transition (Figure 1c). When

$$B = B_{SFI} = M_0(2J-2D+\gamma), \quad (10)$$

$\beta = \frac{\pi}{2}$, implying a spin-flipped (SFID) state (Figure 1d). Therefore, the SFI transition field B_{SFI} depends not only on the moment size M_0 but also on the values of J, γ and D.

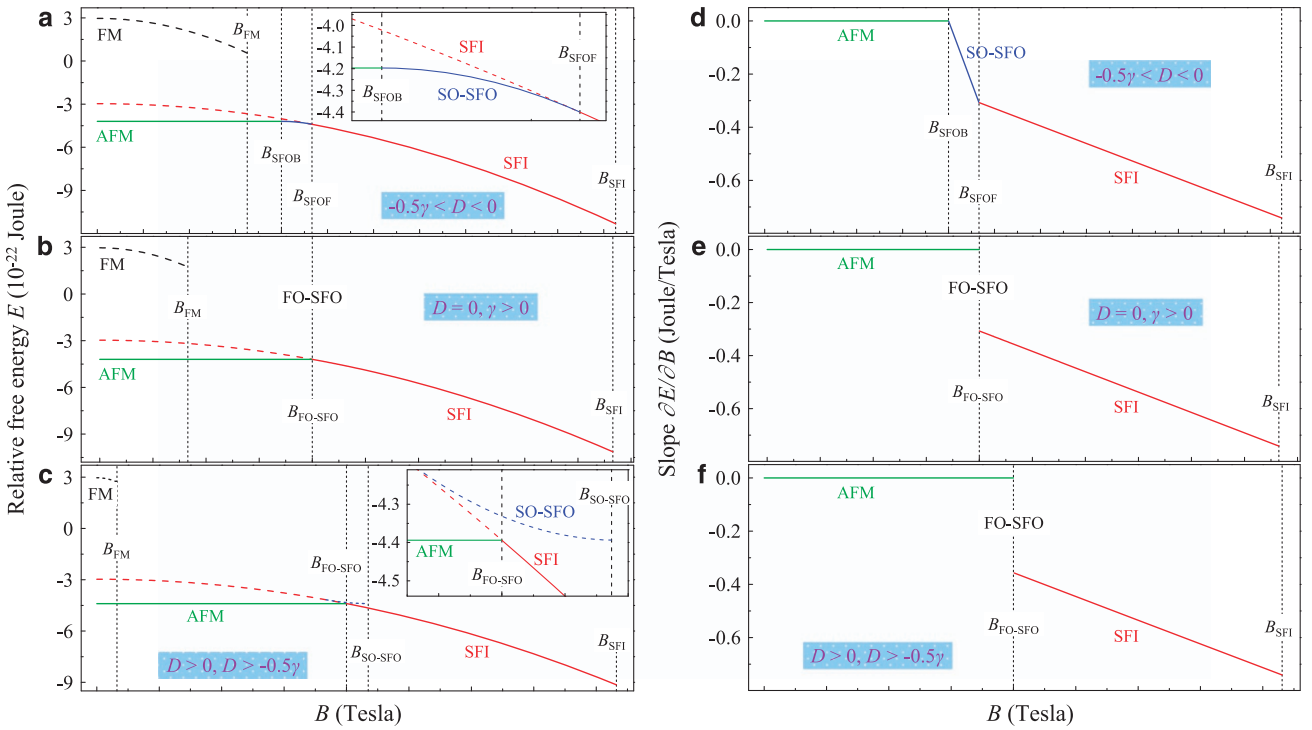

Figure 2. Calculated relative sublattice-moment-related free energies of the deduced magnetic states and the corresponding variations of the free energy slopes, $\partial E/\partial B$, as a function of magnetic field B. (**a**) When $-\frac{1}{2}\gamma < D < 0$, a SO SFO transition occurs. Here we suppose that $M_0 = 4\ \mu_B$, $J = 2\ \mathrm{T}/\mu_B$, $D = -0.2\ \mathrm{T}/\mu_B$ and $B_{SFOB} = 8$ T. (**b**) When $D = 0$ and $\gamma > 0$, a FO SFO transition happens. Here we suppose that $M_0 = 4\ \mu_B$, $J = 2\ \mathrm{T}/\mu_B$, $D = 0\ \mathrm{T}/\mu_B$ and $B_{SFOB} = 8$ T. (**c**) When $D > 0$ and $D > -\frac{1}{2}\gamma$, a FO SFO transition occurs. Here we suppose that $M_0 = 4\ \mu_B$, $J = 2\ \mathrm{T}/\mu_B$, $D = 0.2\ \mathrm{T}/\mu_B$ and $B_{SFOB} = 8$ T. In **a**–**c**, the calculated free energies are all plotted for a clear comparison. The insets of **a**, **c** show an enlargement of the most interesting magnetic-field regimes. The E_{SFI} under $B < B_{SFOF}$ is also shown (dashed read line, as marked). In **c**, the mathematically permissible E of the SO SFO transition is also displayed. In any case, the solid lines as shown in **a**–**c** represent the theoretically allowed magnetic ground states and associated magnetic phase transitions with a change in the strength of magnetic field B. (**d**) When $-\frac{1}{2}\gamma < D < 0$, the first derivative of the sublattice-moment-related free energy E with regard to magnetic field B equals to zero in the AFM state and displays a continuous change while undergoing the SO SFO transition from B_{SFOB} to B_{SFOF} and then the SFI transition from B_{SFO} to B_{SFI}. (**e**) When $D = 0$ and $\gamma > 0$, and (**f**) $D > 0$ and $D > -\frac{1}{2}\gamma$, an abrupt change in the slope occurs at the FO SFO transition field $B_{FO\text{-}SFO} = B_{SFO}$.

(iii) From the combination (3), one can deduce that

$$\beta = \tfrac{\pi}{2}, \text{ and } \sin\phi = \tfrac{B}{M_0(\gamma - 2D)}. \tag{11}$$

When $\beta = \frac{\pi}{2}$, both sublattice moments M_+ and M_- are perpendicular to the AFM axis $M_-^0 M_+^0$, forming a rotating (with magnetic field ***B***) FM-like state. The value of ϕ can intrinsically be modified by a change in magnetic field B.

(iv) The simplest combination (4) indicates $\phi = \beta = \frac{\pi}{2}$, which corresponds to a SFID state as schematically shown in Figure 1d.

Free energy calculations

To calculate free energy scales of the deduced magnetic states from the four combinations (1–4), one can substitute their respective equilibrium phase conditions as discussed above back into Equation (28) and then obtain:

$$E_{AFM(z-axis)} = -(J + \gamma + 2D)M_0^2 \ (0 \le B < B_{SFO}); \tag{12}$$

$$E_{x-axis} = -JM_0^2 (\phi = 90^\circ, \beta = 0^\circ); \tag{13}$$

$$E_{SFI} = -JM_0^2 - \frac{B^2}{2J - 2D + \gamma} (B_{SFO} \le B < B_{SFI}); \tag{14}$$

$$E_{SFID} = (-3J + 2D - \gamma)M_0^2 = [-J - (2J - 2D + \gamma)] M_0^2 (B = B_{SFI}); \tag{15}$$

$$E_{FM-like} = JM_0^2 - \frac{B^2}{\gamma - 2D} [0 \le B \le M_0(\gamma - 2D)]; \tag{16}$$

the one corresponding to the deduced SO SFO transition (Figure 1b) is presented individually as below due to its complexity:

$$E_{SO-SFO} = -JM_0^2(1 - 2\sin^2\beta) - \gamma M_0^2(1 - \sin^2\beta - \delta^2 \sin^2\beta) - DM_0^2 [1 + (1 - 2\delta^2 \sin^2\beta)(1 - 2\sin^2\beta)] - 2BM_0\delta \sin^2\beta$$
$$(\sin\beta = \sqrt{\frac{\delta M_0(2D + \gamma) - B}{4\delta M_0 D}}, \delta = \sqrt{\frac{2J + 2D + \gamma}{2D + \gamma}};$$
$$-\frac{1}{2}\gamma < D < 0; B_{SFOB} \le B < B_{SFOF}). \tag{17}$$

To quantitatively compare the free energies, Equations (12, 13, 14, 15, 16, 17) in the following the comparison will be divided into three parts based on the value of D.

(i) First, the case of the SO SFO transition under the phase condition $-\frac{1}{2}\gamma < D < 0$ is presented. Supposing that $M_0 = 4\ \mu_B$, $J = 2\ \mathrm{T}/\mu_B$, $D = -0.2\ \mathrm{T}/\mu_B$ and $B_{SFOB} = 8$ T,[28,60] which are all substituted into Equation (7), one thus gets $\gamma \sim 1.228\ \mathrm{T}/\mu_B$ that satisfies the boundary condition $D > -\frac{1}{2}\gamma$. Therefore, based on these values, one can obtain that $B_{SFOF} \sim 9.325$ T (Equation (8)), $\delta \sim 2.414$ (Equation (6)) and $B_{SFI} \sim 22.514$ T (Equation (10)). Hence, the relative sublattice-moment-

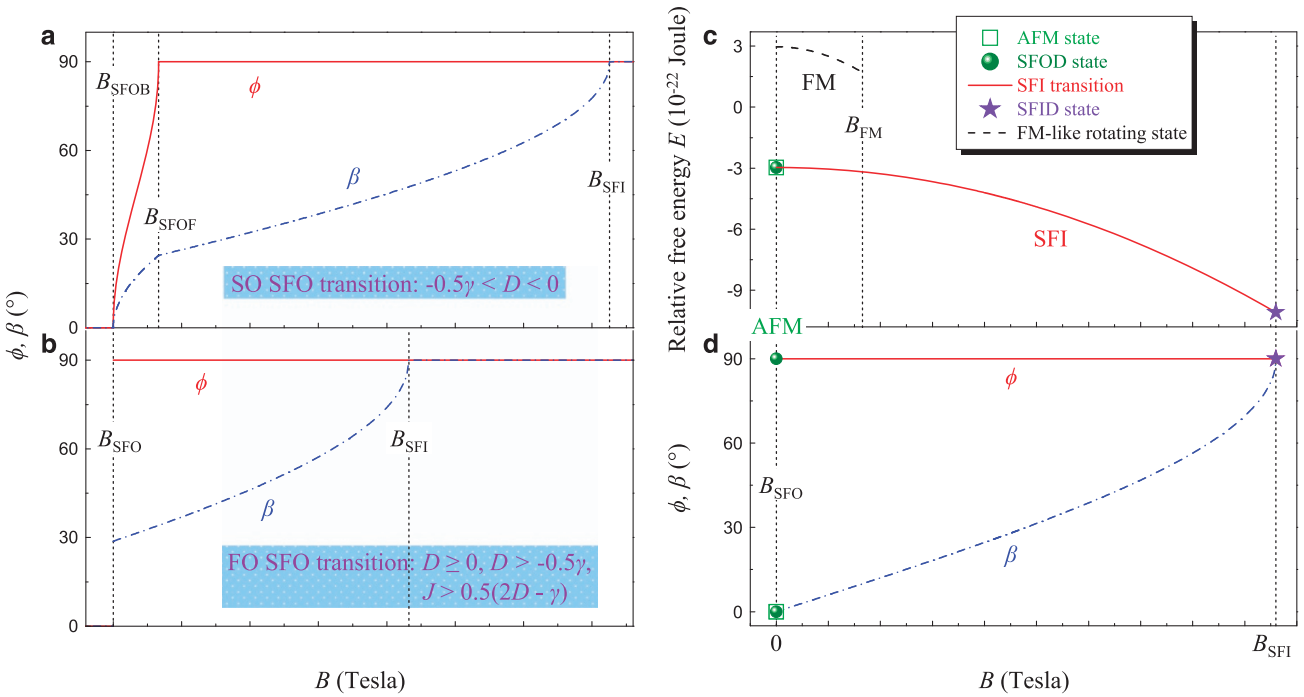

Figure 3. Variations of the angles ϕ and β with magnetic filed B and a direct SFI transition from the AFM state and the corresponding change of the angles ϕ and β when $D=-\frac{1}{2}\gamma$ and $J>-\gamma$, corresponding to Figure 4d. (**a**) When $-\frac{1}{2}\gamma<D<0$, ϕ and β increase continuously in the range of magnetic fields $B_{SFOB}\leqslant B<B_{SFOF}$, suggesting a SO SFO transition. When $B_{SFO}\leqslant B\leqslant B_{SFI}$, $\phi=90°$, and β keeps a continuous increase up to 90° at B_{SFI}. (**b**) When $D\geqslant 0$ and $D>-\frac{1}{2}\gamma$, ϕ suddenly increases up to 90° at $B_{SFOB}=B_{SFOF}=B_{SFO}$ indicative of a FO SFO transition, after which the magnetic phase enters into the process of a SFI transition. In **a**, **b**, below B_{SFOB} (B_{SFO}), $\phi=\beta=0°$; above B_{SFI}, $\phi=\beta=90°$. (**c**) The calculated relative sublattice-moment-related free energies when $D=-\frac{1}{2}\gamma$ and $J>-\gamma$. In this case, $B_{SFO}=0$, and thus a SFI transition occurs directly while $B>0$. (**d**) The corresponding variations of the angles ϕ and β with magnetic field B. In **c**, **d**, $M_0=4$ μ_B, $J=2$ T/μ_B, $D=-0.2$ T/μ_B and $\gamma=0.4$ T/μ_B.

related free energies of all possible magnetic states can be calculated as shown in Figure 2a.

(ii) Second, with the above-assumed parameters, if one sets $D=0$ T/μ_B, then $\gamma\sim0.828$ T/μ_B and $B_{SFOF}=B_{SFOB}=8$ T, which corresponds to a FO SFO transition. The calculated relative free energies at $D=0$ T/μ_B are shown in Figure 2b.

(iii) Third, in the case of $D>0$, $B_{SFOB}>B_{SFOF}$. To extract the exact field for the FO SFO transition, solving E_{AFM} (Equation (12)) = E_{SFI} (Equation (14)) yields that

$$B_{SFO}=M_0\sqrt{(2D+\gamma)(2J-2D+\gamma)}. \quad (18)$$

If one sets $D=0.2$ T/μ_B, then $\gamma\sim0.561$ T/μ_B and $B_{SFI}\sim16.645$ T. The corresponding free energy scales at $D=0.2$ T/μ_B are displayed in Figure 2c.

Nature of the SFO and SFI transitions

As shown in Figure 2a, an AFM state persists up to B_{SFOB}, then a SO SFO transition occurs in the range of magnetic fields $B_{SFOB}\leqslant B\leqslant B_{SFOF}$, followed by a SFI transition at $B>B_{SFOF}$. Finally, all sublattice spins are aligned along the magnetic field direction at B_{SFI}. By contrast, as shown in Figure 2b,c, an antiferromagnet experiences a FO SFO transition at $B_{FO\text{-}SFO}$ and then enters directly into the process of a SFI transition. It is pointed out that an occurrence of the SFO transition is attributed to the existence of magnetic anisotropy, γ and/or D. In the SFOD state,

$$\sin\beta=\frac{B_{SFO}(\text{or } B_{SFOF})}{M_0(2J-2D+\gamma)}. \quad (19)$$

Therefore, the angle β can never be zero, which is a sharp contrast to the traditional FO-type SFO transition, where $\beta=90°$ in the SFOD state.

We calculate the angles ϕ and β, and further confirm the FO and SO SFO transitions. The nature of a SFO transition can also be recognised by the character, continuous or discontinuous, of the first derivative of the free energy (Figure 2) with regard to magnetic field based on the Ehrenfest's criterion[61] for the FO and the SO phase transitions. A continuous slope change is clearly illustrated in Figure 2d, where one can easily deduce that the second derivative ∂^2E/∂^2B is indeed discontinuous. By contrast, an abrupt change in the slope is obviously displayed at B_{FO-SFO} in Figure 2e,f. To better understand the magnetic phase transitions with field, the values of the angles ϕ and β (Figure 1) for all deduced magnetic states are calculated in the whole magnetic field range as shown in Figure 3a,b. The SO (Figure 3a) and FO (Figure 3b) SFO transitions are much clear in terms of the variations of ϕ and β with magnetic field. Until now, it can convincingly be concluded that a SO SFO transition indeed exists theoretically.

DISCUSSION

Equilibrium phase conditions of the magnetic states and nature of the magnetic phase transitions

We first rule out the rotating FM-like state. It is clear that in the magnetic-field range $B\leqslant B_{FM}$, the relative sublattice-moment-related free energy $E_{FM-like}$ is always higher than those of other allowed magnetic states (Figure 2), indicating that the rotating FM-like state does not exist at all in view of its relatively higher free energy.

To clearly present the deduced magnetic ground states and associated magnetic phase transitions with magnetic field, we calculate the three-dimensional (J, γ and D) and the two-dimensional (γ and D) phase diagrams as shown in the up

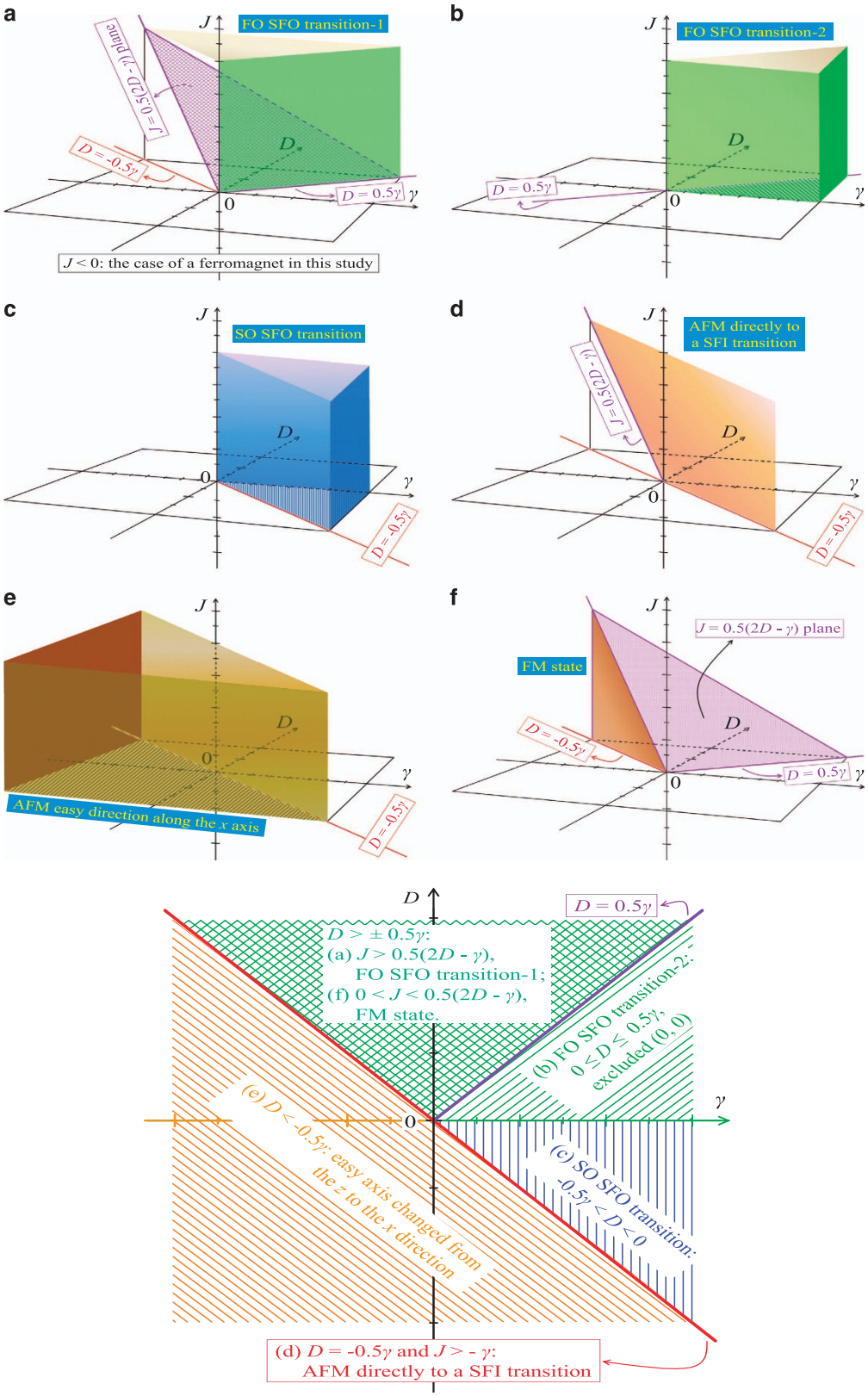

Figure 4. Three-dimensional (J, γ and D; up panel **a**–**f**) and two-dimensional (γ and D; down panel) phase diagrams of a collinear two-sublattice antiferromagnet. (**a**) When $D > \pm 0.5\gamma$ and $J > \frac{1}{2}(2D-\gamma)$, a FO SFO transition 1 occurs. (**b**) When $0 \leqslant D \leqslant 0.5\gamma$, a FO SFO transition 2 occurs. It is pointed out that here γ and D cannot be zero simultaneously. (**c**) When $-\frac{1}{2}\gamma < D < 0$, a SO SFO transition occurs. (**d**) When $D = -\frac{1}{2}\gamma$ and $J > -\gamma$, there is no SFO transition occurring at all. In this case, the antiferromagnet in question goes directly to a SFI transition from the AFM state, and the xz plane becomes an AFM easy plane. (**e**) When $D < -\frac{1}{2}\gamma$, the AFM easy axis changes automatically from the z to the x direction. (**f**) When $D > \pm 0.5\gamma$ and $0 < J < \frac{1}{2}(2D-\gamma)$, the magnet hosts a FM state albeit with an AFM magnetic exchange.

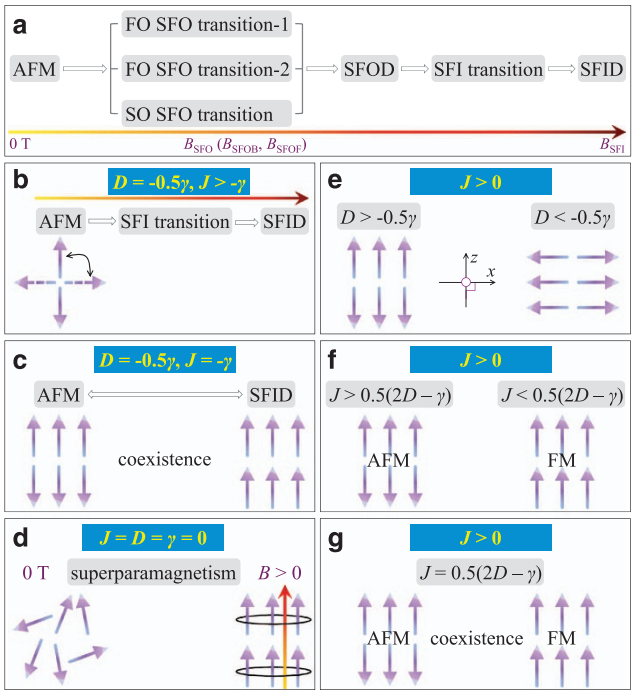

Figure 5. Mathematically allowed magnetic states of a collinear two-sublattice antiferromagnet as a function of J, γ, D and B. (**a**) As magnetic field B increases from 0 to B_{SFO} (for a FO SFO transition) or to B_{SFOB} and B_{SFOF} (for a SO SFO transition) and then to B_{SFI}, the antiferromagnet transfers from an AFM ground state to a FO SFO transition 1 or a FO SFO transition 2 or a SO SFO transition, and then to a SFOD state, from where a SFI transition occurs until all spins are flipped by applied magnetic field. (**b**) When $D = -\frac{1}{2}\gamma$ and $J > -\gamma$, there exists an AFM easy plane. (**c**) When $D = -\frac{1}{2}\gamma$ and $J = -\gamma$, the SFID state has the same energy level as that of the AFM ground state. (**d**) Based on the above analysis of **b**, **c**, one can deduce that when $J = D = \gamma = 0$, if magnetic field $B > 0$ applied, all spins will directly go to the SFID state and point to the applied-field direction. This is the so-called superparamagnetism. (**e**) When $J > 0$ and $D > -\frac{1}{2}\gamma$, the AFM easy axis is along the z direction, whereas when $D < -\frac{1}{2}\gamma$, the x axis becomes an AFM easy direction. (**f**) When $J > 0$ and $J > \frac{1}{2}(2D - \gamma)$, the magnet houses an AFM state, whereas when $J < \frac{1}{2}(2D - \gamma)$, the spins are ferromagnetically arranged. (**g**) When $J > 0$ and $J = \frac{1}{2}(2D - \gamma)$, it is reasonable to deduce that the AFM state coexists with the FM state.

and down panels of Figure 4, respectively. The corresponding spin configurations in point are schematically exhibited in Figure 5.

In this study, for an antiferromagnet $J > 0$. When $J < 0$, on the other hand, the magnet houses a FM state (Figures 4a,f and 5f). In addition, for the existences of the SFO (FO or SO) and SFI transitions, $B_{SFOF} > 0$ (Figure 1b; Equation (20)), $B_{SFO} > 0$ (Figure 1c; Equation (22)) and $B_{SFI} > 0$ (Figure 1d; Equations (20) and (22)). One thus deduce that $J > \frac{1}{2}(2D - \gamma)$ for the validation of these magnetic states. Furthermore, by comparing Equation (12) with Equation (15), one can finally conclude that there exists the possibility for a FM state even when $J > 0$, as shown in Figures 4f and 5f, where $0 < J < \frac{1}{2}(2D - \gamma)$.

From foregoing remarks, we know that for a FO SFO transition, $D \geqslant 0$ and $D > -\frac{1}{2}\gamma$. By including the condition of $J > \frac{1}{2}(2D - \gamma)$ for the validated existence of an antiferromagnet, one can divide the FO SFO transition into two regimes:

(i) FO SFO transition 1: $D > \pm\frac{1}{2}\gamma$ and $J > \frac{1}{2}(2D - \gamma)$ (Figures 1c and 4a);

(ii) FO SFO transition 2: $0 \leq D \leq \pm\frac{1}{2}\gamma$ (Figures 1c and 4b).

In addition, for a SO SFO transition, $-\frac{1}{2}\gamma < D < 0$ (Figures 1b and 4c). It is pointed out that when $-\frac{1}{2}\gamma < D < \frac{1}{2}\gamma$, it is always true that $J > \frac{1}{2}(2D - \gamma)$. The difference between the two types of FO SFO transitions (1 and 2) in the context of J is that for the FO SFO transition 1, $J > 0$ and $J > \frac{1}{2}(2D - \gamma)$; by contrast, for the FO SFO transition 2, J can be any values larger than zero. As shown in Figure 4d, when $D = -\frac{1}{2}\gamma$, $B_{SFOB} = B_{SFOF} = 0$ (Equation (20)). Therefore, the antiferromagnet directly enters a SFI transition (Figure 5b). To further demonstrate this interesting magnetic phase transition, we calculate the relative free energies and the variations of the angles ϕ and β (with the parameters $M_0 = 4\ \mu_B$, $J = 2\ T/\mu_B$, $D = -0.2\ T/\mu_B$ and $\gamma = 0.4\ T/\mu_B$) as shown in Figure 3c,d. It is clear that this magnetic phase transition is theoretically favourable. It is more interesting that if $J = -\gamma$, Equation (12) = Equation (15), which implies that the AFM state can coexist with the SFID state (Figure 5c,g). Based on the above discussion, it is reasonable to deduce that when $J = 0$ (a paramagnetic state) and $D = \gamma = 0$ (without any magnetic anisotropy), all paramagnetic spins will direct and be bounded to an applied-field direction when $B > 0$ (Figure 5d). This is the so-called superparamagnetic state.

When $D < -\frac{1}{2}\gamma$, E_{AFM} (Equation (12)) is always larger than $E_{x\text{-axis}}$ (Equation (13)), which indicates that the AFM easy axis will change from the z to the x direction (Figures 4e and 5e). Therefore, the AFM easy direction is determined by the competition between magnetic anisotropies, γ and D.

An alternative method of estimating the magnetic exchange parameters (J, γ and D)

As foregoing remarks, when $-\frac{1}{2}\gamma < D < 0$ (Figure 1b), a SO SFO transition occurs in the antiferromagnet. With the known exchange parameters (J, γ and D), one can calculate the SFO (B_{SFOB} and B_{SFOF}) and SFI (B_{SFI}) fields, i.e.,

$$\begin{cases} B_{SFOB} = M_0\sqrt{(2D+\gamma)(2J+2D+\gamma)}, \\ B_{SFOF} = M_0(2J-2D+\gamma)\sqrt{\frac{2D+\gamma}{2J+2D+\gamma}}, \\ B_{SFI} = M_0(2J-2D+\gamma). \end{cases} \tag{20}$$

On the other hand, if the values of B_{SFOB}, B_{SFOF} and B_{SFI} are known, one can calculate the corresponding values of J, γ and D according to the following deduced equations from the above Equation 20, i.e.,

$$\begin{cases} D = \frac{B_{SFI}}{4M_0}\left(\frac{B_{SFOB}-B_{SFOF}}{B_{SFOF}}\right), \\ \gamma = \frac{1}{M_0}\left[\frac{B_{SFOB}B_{SFOF}}{B_{SFI}} - \frac{B_{SFI}(B_{SFOB}-B_{SFOF})}{2B_{SFOF}}\right], \\ J = \frac{1}{2M_0}\left[B_{SFI} - \frac{B_{SFOB}B_{SFOF}}{B_{SFI}} + \frac{B_{SFI}(B_{SFOB}-B_{SFOF})}{B_{SFOF}}\right]. \end{cases} \tag{21}$$

When $D \geqslant 0$, $D > -\frac{1}{2}\gamma$ and $J > \frac{1}{2}(2D - \gamma)$ (Figure 1c), a FO SFO transition occurs, and

$$\begin{cases} B_{SFO} = M_0\sqrt{(2D+\gamma)(2J-2D+\gamma)}, \\ B_{SFI} = M_0(2J-2D+\gamma). \end{cases} \tag{22}$$

Although it is impossible to solve the above Equation 22 to extract the detailed values of J, γ and D, one can deduce that

$$2D + \gamma = \frac{B_{SFO}^2}{M_0 B_{SFI}}. \tag{23}$$

Hence, one can calculate two special cases, i.e.,

$$\begin{cases} \text{if } D = 0 \\ \text{then } \gamma = \frac{B_{SFO}^2}{M_0 B_{SFI}}, \text{ and} \\ J = \frac{B_{SFI}^2 - B_{SFO}^2}{2M_0 B_{SFI}}; \end{cases} \tag{24}$$

and

$$\begin{cases} \text{if } \gamma = 0 \\ \text{then } D = \frac{B_{SFO}^2}{2M_0 B_{SFI}}, \text{ and} \\ J = \frac{B_{SFI}^2 + B_{SFO}^2}{2M_0 B_{SFI}}. \end{cases} \tag{25}$$

Traditionally, through fitting the relevant ***Q*** (momentum)–*E* (energy) spectra recorded usually by inelastic neutron scattering, one can extract the magnetic exchange parameters (*J*, *γ* and *D*). Here based on our model, one can first obtain the values of B_{SFO} (B_{SFOB} and B_{SFOF}) and B_{SFI} for a suitable SFO and SFI compound, e.g., via magnetisation measurements using a commercial physical property measurement system or a Quantum Design MPMS-7 SC quantum interference device magnetometer (San Diego, CA, USA). Then, the values of *J*, *γ* and *D* can be estimated according to Equations (21), (24) or (25).

CONCLUSIONS

In summary, a consistent mean-field calculation of the SFO and SFI phase transitions has been performed for localised collinear antiferromagnets with two sublattices. In this study, we can unify all possible magnetic ground states as well as related magnetic phase transitions within one model. Some special magnetic states are derived with a change in the strength of magnetic field:

(i) A rotating FM-like state (that is finally ruled out);
(ii) A SO SFO transition;
(iii) A direct SFI transition from the AFM state without experiencing a SFO transition as usual;
(iv) An existence of the FM state;
(v) A coexistence of the AFM and FM states even when the magnetic exchange is of AFM.

Based on the quantitative changes of the ground-state free energies, the case (i) has been clearly ruled out, and the others indeed exist theoretically. This model calculation unifies the AFM state, FO and SO SFO transitions, SFOD state, SFI transition as well as the SFID state. Their respective phase boundary conditions are extracted and clearly listed. We find an alternative to the estimation of magnetic exchange parameters (*J*, *γ* and *D*). Inelastic neutron scattering studies of suitable real SFO and SFI compounds to extract the relevant parameters for an experimental verification of the phase boundary conditions and especially the studies in the intermediate coupling regimes to explore possible quantum fluctuations will be of great interest and challenge, and Equation (28) merits a tentative expansion with more agents such as temperature and an angle denoting the misalignment between AFM axis and applied magnetic field direction.

MATERIALS AND METHODS

The calculation presented here is limited to purely localised collinear AFM systems, ignoring the effect of valence electrons on magnetic couplings. For a two-sublattice AFM spin configuration (Figure 1), the corresponding Hamiltonian terms consist principally of magnetic exchange, spin-exchange anisotropy, single-ion anisotropy and Zeeman coupling to an external magnetic field. Assuming that an AFM easy direction consistent with the localised sublattice moments M_+ and M_- is along the *z* axis (Figure 1a) and that the subsequent completely flopped spins are parallel to the *x* axis (Figure 1b and c), the sublattice-moment vectors within the *xz* plane (Figure 1b) can thus be written as:

$$\begin{cases} \widehat{M_+} = M_+[\hat{x}\sin(\phi-\beta_1)+\hat{z}\cos(\phi-\beta_1)] \text{ and} \\ \widehat{M_-} = -M_-[\hat{x}\sin(\phi+\beta_2)+\hat{z}\cos(\phi+\beta_2)], \end{cases} \quad (26)$$

respectively, where $\hat{x}$ and $\hat{z}$ are the unit vectors along the *x* and *z* axes, respectively, and the angles ϕ, β_1 and β_2 are defined as marked in Figure 1. Therefore, the resultant sublattice-moment-related free energy (*E*) within a mean-field approximation can be calculated by:

$$\begin{aligned} E &= JM_+\cdot M_- + \gamma M_+^z M_-^z - D\left[(M_+^z)^2+(M_-^z)^2\right] - B(M_+^z+M_-^z) \\ &= -JM_+M_-\cos(\beta_1+\beta_2)-\gamma M_+M_-\cos(\phi-\beta_1)\cos(\phi+\beta_2) \\ &\quad -D\left[M_+^2\cos^2(\phi-\beta_1)+M_-^2\cos^2(\phi+\beta_2)\right] \\ &\quad -B[M_+\cos(\phi-\beta_1)-M_-\cos(\phi+\beta_2)], \end{aligned} \quad (27)$$

where the four terms in turn denote the four Hamiltonian components as the foregoing remarks, and J (>0), γ and D are the AFM coupling, anisotropic exchange and single-ion anisotropic energies, respectively. In an unsaturation magnetic state, with increasing magnetic field ***B*** ($\|$ *z* axis) as shown in Figure 1a,b, the sublattice moment M_+ (M_-) increases (decreases) as a consequence, which leads to $\beta_1<\beta_2$. At the lowest temperature $T=0$ K, i.e., in a real saturation magnetic state, $M_+\equiv M_-=M_0$ and thus $\beta_1\equiv\beta_2=\beta$. Hence, Equation (27) can be simplified as:

$$\begin{aligned} E &= JM_0^2\cos(2\beta)-\gamma M_0^2\cos(\phi-\beta)\cos(\phi+\beta) \\ &\quad -DM_0^2\left[\cos^2(\phi-\beta)+\cos^2(\phi+\beta)\right] \\ &\quad -BM_0^2[\cos(\phi-\beta)-\cos(\phi+\beta)] \\ &= -JM_0^2\cos(2\beta)-\frac{\gamma M_0^2}{2}[\cos(2\phi)+\cos(2\beta)] \\ &\quad -DM_0^2[1+\cos(2\phi)\cos(2\beta)]-2BM_0\sin\phi\sin\beta. \end{aligned} \quad (28)$$

ACKNOWLEDGEMENTS

H.-F. Li acknowledges the start-up research grant at the University of Macau.

CONTRIBUTIONS

H.-F. Li led the project and wrote the paper.

COMPETING INTERESTS

The author declares no conflict of interest.

REFERENCES

1. Van Santen, J. H. & Jonker, G. H. Electrical conductivity of ferromagnetic compounds of manganese with perovskite structure. *Physica* **16**, 599–600 (1950).
2. Bednorz, J. G. & Muller, K. A. Possible high T_c superconductivity in the Ba-La-Cu-O system. *Z. Phys. B* **64**, 189–193 (1986).
3. Jin, S. *et al.* Thousandfold change in resistivity in magnetoresistive La-Ca-Mn-O films. *Science* **264**, 413–415 (1994).
4. Fiebig, M., Lottermoser, Th., Fröhlich, D., Goltsev, A. V. & Pisarev, R. V. Observation of coupled magnetic and electric domains. *Nature* **419**, 818–820 (2002).
5. Kimura, T. *et al.* Magnetic control of ferroelectric polarization. *Nature* **426**, 55–58 (2003).
6. Eerenstein, W., Mathur, N. D. & Scott, J. F. Multiferroic and magnetoelectric materials. *Nature* **442**, 759–765 (2006).
7. Monthoux, P., Pines, D. & Lonzarich, G. G. Superconductivity without phonons. *Nature* **450**, 1177–1183 (2007).
8. Cheong, S. W. & Mostovoy, M. Multiferroics: a magnetic twist for ferroelectricity. *Nat. Mater.* **6**, 13–20 (2007).
9. Paglione, J. & Greene, R. L. High-temperature superconductivity in iron-based materials. *Nat. Phys.* **6**, 645–658 (2010).
10. Greiner, M., Mandel, O., Esslinger, T., Hänsch, T. W. & Bloch, I. Quantum phase transition from a superfluid to a Mott insulator in a gas of ultracold atoms. *Nature* **415**, 39–44 (2002).
11. Senthil, T., Vishwanath, A., Balents, L., Sachdev, S. & Fisher, M. P. A. Deconfined quantum critical points. *Science* **303**, 1490–1494 (2004).
12. Coleman, P. & Schofield, A. J. Quantum criticality. *Nature* **433**, 226–229 (2005).
13. Rønnow, H. M. *et al.* Quantum phase transition of a magnet in a spin bath. *Science* **308**, 389–392 (2005).
14. Zwierlein, M. W., Schunck, C. H., Schirotzek, A. & Ketterle, W. Direct observation of the superfluid phase transition in ultracold Fermi gases. *Nature* **442**, 54–58 (2006).

15. Sachdev, S. Quantum magnetism and criticality. *Nat. Phys.* **4**, 173–185 (2008).
16. Balakirev, F. F. *et al.* Quantum phase transition in the magnetic-field-induced normal state of optimum-doped high-T_c cuprate superconductors at low temperatures. *Phys. Rev. Lett.* **102**, 017004 (2009).
17. Simon, J. *et al.* Quantum simulation of antiferromagnetic spin chains in an optical lattice. *Nature* **472**, 307–312 (2011).
18. Zyuzin, A. A., Hook, M. D. & Burkov, A. A. Parallel magnetic field driven quantum phase transition in a thin topological insulator film. *Phys. Rev. B* **83**, 245428 (2011).
19. Scott, J. F. Searching for new ferroelectrics and multiferroics: a user's point of view. *npj Comput. Mater.* **1**, 15006 (2015).
20. Chen, L.-Q. *et al.* Design and discovery of materials guided by theory and computation. *npj Comput. Mater.* **1**, 15007 (2015).
21. Kirklin, S. *et al.* The Open Quantum Materials Database (OQMD): assessing the accuracy of DFT formation energies. *npj Comput. Mater.* **1**, 15010 (2015).
22. Yang, J. *et al.* On the tuning of electrical and thermal transport in thermoelectrics: an integrated theory-experiment perspective. *npj Comput. Mater.* **2**, 15015 (2016).
23. Urban, A., Seo, D.-H. & Ceder, G. Computational understanding of Li-ion batteries. *npj Comput. Mater.* **2**, 16002 (2016).
24. Néel, L. Propriétés magnétiques de l'état magnétique et énergie d'interaction entre atomes magnétiques. *Ann. de Phys.* **5**, 232–279 (1936).
25. Poulis, N. J., van den Handel, J., Ubbink, J., Poulis, J. A. & Gorter, C. J. On antiferromagnetism in a single crystal. *Phys. Rev.* **82**, 552 (1951).
26. Anderson, F. B. & Callen, H. B. Statistical mechanics and field-induced phase transitions of the Heisenberg antiferromagnet. *Phys. Rev.* **136**, A1068–A1087 (1964).
27. Ranicar, J. H. & Elliston, P. R. Spin-flopping in $LiMnPO_4$ and Cr_2BeO_4. *Phys. Lett.* **25A**, 720–721 (1967).
28. Toft-Petersen, R. *et al.* Magnetic phase diagram of magnetoelectric $LiMnPO_4$. *Phys. Rev. B* **85**, 224415 (2012).
29. Tian, W. *et al.* Neutron scattering studies of $LiCoPO_4$ & $LiMnPO_4$. *J. Phys. Conf. Ser.* **251**, 012005 (2010).
30. Schelleng, J. H. & Friedberg, S. A. Thermal behavior of the antiferromagnet $MnBr_2{\cdot}4H_2O$ in applied magnetic fields. *Phys. Rev. B* **185**, 728–734 (1969).
31. Shapira, Y. & Foner, S. Magnetic phase diagram of MnF_2 from ultrasonic and differential magnetization measurements. *Phys. Rev. B* **1**, 3083–3096 (1970).
32. Rohrer, H. Properties of $GdAlO_3$ near the spin-flop bicritical point. *Phys. Rev. Lett.* **34**, 1638–1641 (1975).
33. Butera, R. A., Corliss, L. M., Hastings, J. M., Thomas, R. & Mukamel, D. Neutron scattering investigation of the spin-flop transition in $MnCl_2{\cdot}4D_2O$. *Phys. Rev. B* **24**, 1244–1254 (1981).
34. Paduan-Filho, A., Becerra, C. C. & Palacio, F. Hysteresis at the spin-flop transition in the antiferromagnets $K_2Fe(Cl_{1-x}Br_x)_5{\cdot}H_2O$. *Phys. Rev. B* **43**, 11107–11111 (1991).
35. Bogdanov, A. N., Zhuravlev, A. V. & Rößler, U. K. Spin-flop transition in uniaxial antiferromagnets: magnetic phases, reorientation effects, and multidomain states. *Phys. Rev. B* **75**, 094425 (2007).
36. Holmes, L., Eibschütz, M. & Guggenheim, H. J. SPIN-FLOP TRANSITION IN $BaMnF_4$. *Solid State Commun.* **7**, 973–976 (1969).
37. Saito, H., Suzuki, S., Fukamichi, K., Mitamura, H. & Goto, T. Metamagnetic transition in GdSi. *J. Phys. Soc. Jpn* **65**, 1938–1940 (1996).
38. Wolf, M., Ruck, K., Eckert, D., Krabbes, G. & Müller, K. H. Spin-flop transition in the low-dimensional compound $Ba_3Cu_2O_4Cl_2$. *J. Magn. Magn. Mater.* **196–197**, 569–570 (1999).
39. Tsukada, I., Takeya, J., Masuda, T. & Uchinokura, K. Two-Stage Spin-Flop Transitions in the $S=1/2$ Antiferromagnetic Spin Chain $BaCu_2Si_2O_7$. *Phys. Rev. Lett.* **87**, 127203 (2001).
40. Tsukada, I., Takeya, J., Masuda, T., Uchinokura, K. & Zheludev, A. Anomalous two-stage spin-flop transiton in $BaCu_2Si_2O_7$. *Physica B* **329–333**, 886–887 (2003).
41. Zou, J. D., Liu, J. & Yan, M. Crystal structure and magnetic properties of $GdSi_{1.78}$, $Gd(Si_{0.684}Ge_{0.316})_{1.78}$, $GdGe_{1.57}$, and $GdSn_2$ compounds. *J. Magn. Magn. Mater.* **385**, 77–82 (2015).
42. Oliveira, N. F., Paduan Filho, Jr A., Salinas, S. R. & Becerra, C. C. Magnetic phase diagram of $NiCl_2{\cdot}6H_2O$: The low-temperature canted-paramagnetic boundary and the bicritical point. *Phys. Rev. B* **18**, 6165–6177 (1978).
43. Becerra, C. C., Paduan-Filho, A., Palacio, F. & Barbeta, V. B. Random field effects at the spin-flop transition of diluted and mixed $(K_{1-x}Rb_x)_2Fe_{1-y}In_y(Cl_{1-z}Br_z)_5{\cdot}H_2O$. *J. Appl. Phys.* **73**, 5491–5494 (1993).
44. Keffer, F. & Chow, H. Dynamics of the antiferromagnetic spin-flop transition. *Phys. Rev. Lett.* **31**, 1061–1064 (1973).
45. King, A. R. & Rohrer, H. Spin-flop bicritical point in MnF_2. *Phys. Rev. B* **19**, 5864–5876 (1979).
46. Lynn, J. W., Heller, P. & Lurie, N. A. Neutron-diffraction study of the staggered magnetization of $CuCl_2{\cdot}2D_2O$. *Phys. Rev. B* **16**, 5032–5039 (1977).
47. Oh, Y. S. *et al.* Non-hysteretic colossal magnetoelectricity in a collinear antiferromagnet. *Nat. Commun.* **5**, 3201–3207 (2014).
48. Yokosuk, M. O. *et al.* Tracking the continuous spin-flop transition in Ni_3TeO_6 by infrared spectroscopy. *Phys. Rev. B* **92**, 144305 (2015).
49. Smeets, J. P. M., Frikkee, E. & de Jonge, W. J. M. Intermediate phase in a spin-flop system with coupled order parameters. *Phys. Rev. Lett.* **49**, 1515–1518 (1982).
50. Basten, J. A. J., de Jonge, W. J. M. & Frikkee, E. Intermediate phase in the spin-flop system $CoBr_2{\cdot}6(0.48D_2O, 0.52H_2O)$. *Phys. Rev. B* **21**, 4090–4093 (1980).
51. Yamashita, N. Field induced phase transitions in uniaxial antiferromagnets. *J. Phys. Soc. Jpn* **32**, 610–615 (1972).
52. Liu, K. S. & Fisher, M. E. Quantum lattice gas and the existence of a supersolid. *J. Low Temp. Phys.* **10**, 655–683 (1973).
53. Becerra, C. C. & Ferreira, L. G. Phase transitions in uniaxial antiferromagnets. *J. Phys. Soc. Jpn* **37**, 951–955 (1974).
54. Li, H.-F. *et al.* Incommensurate antiferromagnetic order in the manifoldly-frustrated $SrTb_2O_4$ with transition temperature up to 4.28 K. *Front. Phys.* **2**, 42 (2014).
55. Li, H.-F. *et al.* Absence of magnetic ordering in the ground state of a $SrTm_2O_4$ single crystal. *J. Mater. Chem. C* **3**, 7658–7668 (2015).
56. Li, H.-F. *et al.* Magnetization, crystal structure and anisotropic thermal expansion of single-crystal $SrEr_2O_4$. *RSC Adv.* **4**, 53602–53607 (2014).
57. Li, H.-F. *et al.* Distinct itinerant spin-density waves and local-moment antiferromagnetism in an intermetallic $ErPd_2Si_2$ single crystal. *Sci. Rep.* **5**, 7968 (2015).
58. Li, H. *et al.* Possible magnetic-polaron-switched positive and negative magnetoresistance in the GdSi single crystals. *Sci. Rep.* **2**, 750 (2012).
59. Prystasz, W. Phase diagram for the antiferromagnet with the ferromagnetic integral of intersublattice exchange. *Solid State Commun.* **44**, 267–269 (1982).
60. Peters, D., McCulloch, I. P. & Selke, W. Spin-one Heisenberg antiferromagnetic chain with exchange and single-ion anisotropies. *Phys. Rev. B* **79**, 132406 (2009).
61. Tari, A. *The Specific Heat of Matter at Low Temperatures* (Imperial College Press: London, 2003).